Optical Engineering

SPIEDigitalLibrary.org/oe

Proton radiation testing of digital micromirror devices for space applications

Kenneth Fourspring
Zoran Ninkov
Bryan C. Fodness
Massimo Robberto
Sally Heap
Alex G. Kim

Downloaded From: http://opticalengineering.spiedigitallibrary.org/ on 04/25/2016 Terms of Use: http://spiedigitallibrary.org/ss/TermsOfUse.aspx

Proton radiation testing of digital micromirror devices for space applications

Kenneth Fourspring
Zoran Ninkov
Bryan C. Fodness
Rochester Institute of Technology
54 Lomb Memorial Drive
Rochester, New York 14623
E-mail: kdf5036@rit.edu

Massimo Robberto
Space Telescope Science Institute
3700 San Martin Drive
Baltimore, Maryland 21212

Sally Heap
Code 681 NASA Goddard Space Flight Center
Greenbelt, Maryland 20771

Alex G. Kim
Lawrence Berkeley National Laboratory
1 Cyclotron Road
Berkeley, California 94720

Abstract. Scientists are interested in using digital micromirror devices (DMD) as slit-masks in multiobject spectrometers on future space missions. A favored orbit is at the second Lagrangian point (L2). A requirement for mission planning is to determine how long such microelectrical mechanical systems devices would remain operational given the L2 radiation environment, which is primarily composed of solar protons and cosmic rays. To this end, we initiated DMD proton testing. Three DMDs were irradiated with high-energy protons (35 to 50 MeV) at the Lawrence Berkeley National Laboratory 88 in. Cyclotron. Assuming a typical spacecraft shielding of 100 mils of aluminum, our tests imply that DMDs remain fully operable in a five-year mission at L2 with a margin of safety of 4.5. © *2013 Society of Photo-Optical Instrumentation Engineers (SPIE)* [DOI: 10.1117/1.OE.52.9.091807]

Subject terms: digital micromirror devices; microelectrical mechanical systems; proton irradiation.

Paper 130071SS received Jan. 15, 2013; revised manuscript received Apr. 12, 2013; accepted for publication Apr. 16, 2013; published online May 13, 2013.

1 Introduction

1.1 *Digital Micromirror Devices*

Microelectrical mechanical systems (MEMS) are tiny mechanical devices produced with existing semiconductor fabrication techniques that integrate electrical interconnects and drive electronics into a single package. MEMS are the solution for miniaturizing bulky discrete devices and sensors. A miniaturized array of MEMS mirrors, the digital micromirror device (DMD), has been under development at Texas Instruments (TI) for several decades.[1] DMDs modulate light spatially in digital projectors by flipping individual mirrors between two stable orientations. Many studies on DMDs in digital projectors, all yielding favorable results, have been performed to evaluate the long-term reliability and stability of DMDs.[2] The TI DMDs tested in the present work are 0.7 in. 1024×768 exended graphics array (XGA) DMDs, that have a 12-deg. tip angle and a pitch of 13.68. They represent one of TI's current generation devices. Previous studies describing the use of DMDs for multiobject spectrometers (MOS), namely Rochester Institute of Technology multiobject spectrograph (RITMOS)[3] and infrared multiobject spectrograph (IRMOS),[4] utilized an earlier generation DMD that had limited contrast, fewer total mirrors and significant scattered light. Current DMDs have much greater contrast and optical performance due to the increased mirror tip angle, smaller mirror via structure, and a reduced gap between adjacent mirrors [see Fig. 1(a)]. MOS is an acronym for metal oxide semiconductor, which are used in the DMDs' integrated drive circuitry, but in this paper the term MOS will be used to abbreviate the phrase Multiobject Spectroscopy.

The DMD is hermetically encapsulated, which is integral to the device's robustness and reliability. Moisture and particle contamination are problems for un-packaged devices. Figure 1 shows the package structure. The DMD silicon is mounted to a ceramic carrier, and gold wire-bonds are used to connect the silicon chip bond pads. A kovar metal frame is mounted to the ceramic carrier. Another kovar metal frame is fused together with an alkali-borosilicate glass (Corning type 7056 glass) window and electro-welded to the first metal frame. This sealed package is then backfilled with dry nitrogen. The operational temperature of a DMD would likely be somewhere between −40°C to −100°C depending on mission requirements. It is well understood that radiation effects can be highly temperature dependent.[5] However, to keep the test apparatus practical for these initial tests, it was decided to irradiate the DMDs while they operated at room temperature. Future work will discuss testing DMDs at the appropriate operational temperatures.

1.2 *Radiation Tolerant Slit-Mask (Motivation)*

The current ground-based approach to MOS generally uses one of two approaches to separate targets of interest: fibers (e.g., Hydra[6]) or masks [e.g., Gemini multiobject spectrograph (GMOS)[7]]. For Hydra, large mechanical stems position fibers in the telescope focal plane. The re-position times are on the order of an hour, and there are inherent limitations as to the minimum separation between two fibers. For GMOS, the two-step procedure involves capturing an image of the target field that is then used to machine the slit mask. Neither of these approaches are practical for deployment in space.

0091-3286/2013/$25.00 © 2013 SPIE

Downloaded From: http://opticalengineering.spiedigitallibrary.org/ on 04/25/2016 Terms of Use: http://spiedigitallibrary.org/ss/TermsOfUse.aspx

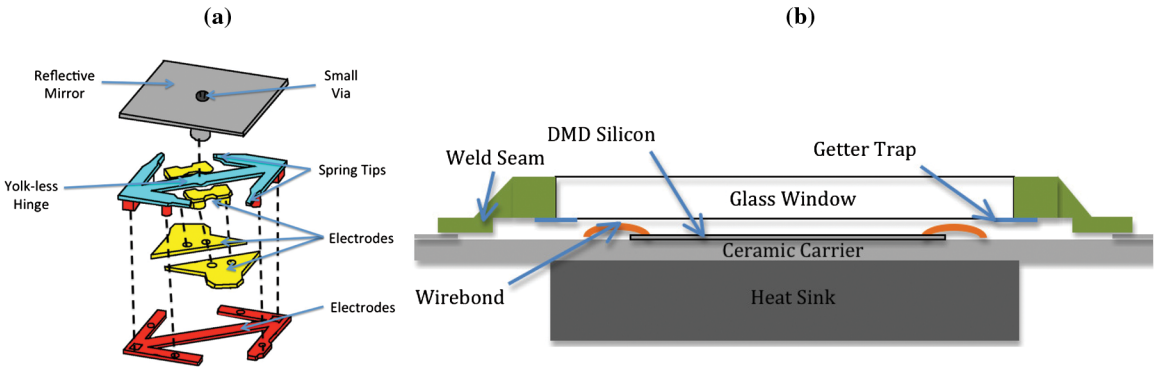

Fig. 1 (a) Illustration shows an extrapolated view of an individual DMD mirror. This mirror architecture is denoted as TI's fast track design. Reflective surface of the mirror is fabricated from an aluminum alloy. (b) Diagram shows a "Type-A" DMD package. The silicon substrate containing the array of DMD mirrors is mounted to a ceramic carrier. Borosilicate window is held above the DMD by a kovar metal frame. Device is wire-bonded to interconnects, which terminate at the bottom of the ceramic carrier.

The James Webb Space Telescope (JWST) includes a multiobject Near InfraRed Spectrometer (NIRSpec)[8] as a primary instrument. The instrument uses a microshutter array (MSA) to define the slits for the spectrometer. The JWST MSA uses 100×200 shutters and was custom built at the NASA Goddard Space Flight Center. These MSAs have limitations due to the high number of defective shutters and small format sizes (365×171). There is great interest to find alternative technologies to make programmable slits for future space missions. The commercial off the shelf (COTS) DMD is a logical candidate to fulfill this role. DMDs are readily available with 100% operability and large format (up to 4000×2000 elements). The mirrors' aluminum surface provides a broad spectral reflectivity. These COTS low cost mirrors are integrated with complementary metal oxide semiconductor (CMOS) circuitry to allow spatial mirror patterns to be uploaded easily.

Two DMD ground-based MOS instruments have been constructed and deployed (RITMOS[3] and IRMOS[4]), and one more is in development (BATMAN[9]). These systems proved to be useful MOS instruments and are precursors for future space experiments.[10] However, one of the outstanding uncertainties is the radiation tolerance of the DMD. Gamma radiation testing has been completed on DMDs with a cumulative gamma dose of 10 to 15 krad–silicon.[11] These results reported some failure modes at this dose. Unfortunately, the DMD and its drive electronics board were both irradiated during this test. It is not possible to unambiguously distinguish whether the DMD or drive electronics was the source of the degraded performance. MEMS components are becoming more commonly used in spacecraft, but radiation testing of these devices is still in its beginnings.[12] This paper reports on the first proton testing of a DMD.

1.3 *Radiation Modeling*

The purpose of proton testing the DMD is to evaluate how it would function in the space environment, especially at L2 (the second Lagrangian point). The L2 orbit is outside the boundary of the Van-Allen Radiation belts, so the primary radiation is composed of solar protons. Cosmic rays (composed of protons, electrons, gamma rays, x-rays and heavy ions) also account for a portion of the radiation exposure at L2. The radiation budget is also a function of the Sun's 11 year cycle. The proton spectrum at L2 was modeled using the space environment information system (SPENVIS) software package.[13] The Emission of Solar Proton (ESP) model[14] was used to predict the long-term solar particle fluence for a five-year mission at L2 assuming a 95% confidence level. Figure 2 shows the shielded proton fluence for a five-year mission at L2 starting in 2020 using the SHIELDDOSE2 model. For a 3-mm-thick borosilicate window the shielding provided by the glass is 2.47 mm of equivalent aluminum. The ratio of borosilicate's density $[2.33(\mathrm{g/cm^3})]$ to aluminum's density $[2.70(\mathrm{g/cm^3})]$ was used to calculate this equivalent thickness. The bottom and sides of the DMD package offer additional shielding beyond that of the window. As shown in Fig. 2, the expected dose at the DMD silicon with just the window as shielding is predicted to be 15 krad. A common value used for the level of space-craft shielding is 100 mils = 2.54 mm of equivalent aluminum.[15] Assuming this additional shielding, the

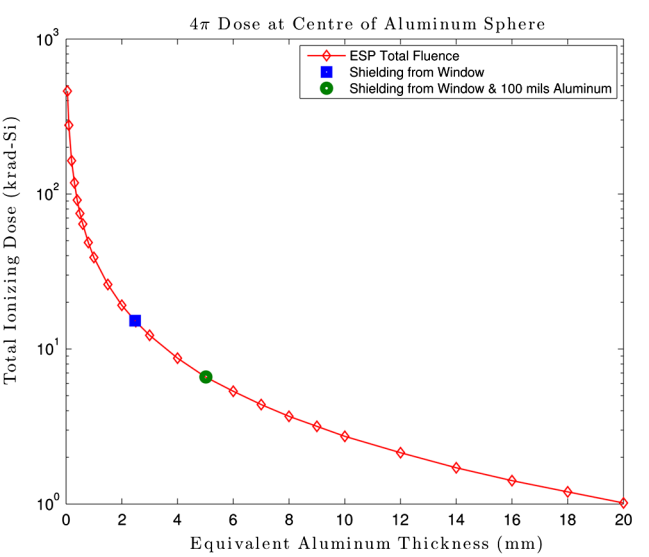

Fig. 2 Total dose of Solar protons in silicon after a five-year mission at L2 (modeled by SPENVIS). 2.47 mm of aluminum shielding corresponds to the shielding provided by the package. Additionally, 100 mil of equivalent aluminum shielding is shown.

Downloaded From: http://opticalengineering.spiedigitallibrary.org/ on 04/25/2016 Terms of Use: http://spiedigitallibrary.org/ss/TermsOfUse.aspx

expected dose at the DMD silicon would be 6.6 krad for a five-year L2 mission. As will be discussed in Sec. 2.4, the DMDs were irradiated to a dose of 40 krad. The range of proton energies (i.e., 35 to 50 MeV) used in the irradiation test were chosen to be near the peak proton fluence (see Fig. 3) at L2.

Proton testing often involves irradiating electronic parts of interest, and assessing both ionizing and nonionizing damage. The effect of proton radiation on an electronic component can also be cumulative or transient in nature. Cumulative effects are proportional to the total ionizing dose (TID). One kind of transient phenomenon is known as single event effects (SEE). There are many different classifications of SEEs, but one of particular interest is single event upsets (SEU). A SEU is a type of soft error, which occurs when an energetic particle passes close to a sensitive node of a memory element, resulting in a flipped bit.

The DMDs were proton tested with their packaging intact, as this is the most likely scenario for deployment in space. Any material (e.g., the DMD window) in the proton beam results in interactions that degrade the beam energy and fluence; however, testing the packaged DMD eliminates the possibility of moisture or particle induced mirror failure. This means that the protons must be accelerated with sufficient energy to pass through the DMD window and interact electrically with the DMD silicon to obtain meaningful results.

The proton flux incident on the DMD window was measured using an ionization chamber. The software package SRIM[16] was used to model the beam energy at the DMD silicon after passage through the window. The results of this modeling are shown in Table 1, which lists the input beam energy, modeled energy at the device and corresponding dose conversion factor (CF). The dose CF using the lower energy linear energy transfer (LET) was used to calculate the dose deposited in the device behind the window. A dose measured incident on the window is then multiplied by the CF to obtain the dose at the DMD silicon behind the window. After the protons pass through the window they have a lower energy, and therefore deposit a greater dose due to the larger LET $(\mathrm{d}E/\mathrm{d}x)$. For example, a 1 krad dose of 34.0 MeV protons incident on the package, corresponds to a 1.4 krad dose of 21.0 MeV protons at the silicon.

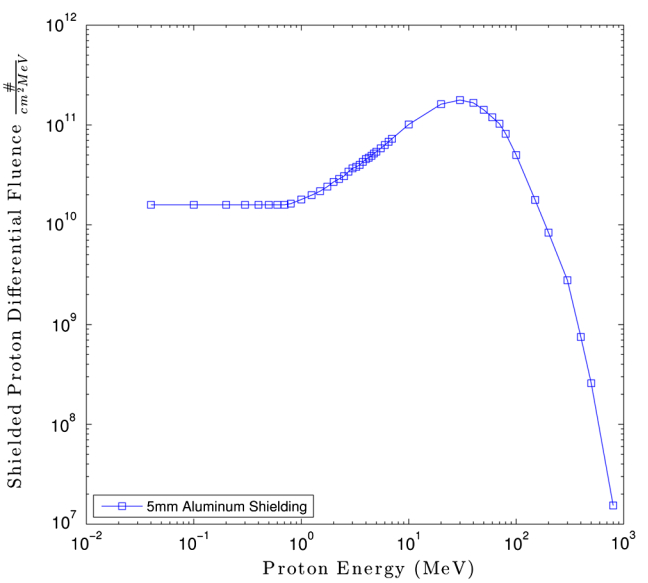

Fig. 3 Proton fluence as a function of energy at L2. Calculated using the ESP solar proton model using a total shielding thickness of 5 mm equivalent aluminum.

Table 1 Beam energy, LET and dose correction factors from SRIM model.

Beam energy (MeV)			LET $\mathrm{d}E/\mathrm{d}x$		
At window	At mirror	ΔEnergy	In window	In silicon	CF
34.0	21.0	13.0	0.0134	0.0189	1.409
44.2	34.5	9.7	0.0109	0.0132	1.214
49.9	40.9	9.0	0.0100	0.0116	1.158

2 Experiment

The experiment was run using the following strategy. Three DMDs were irradiated (Serial numbers 140508, 140507, and 140106) using a different proton energy for each device, 34.0, 44.2, and 49.9 MeV. We will refer in the rest of this paper to the beam energy on the DMD after the window's absorption, i.e., 21.0, 34.5, and 40.9 MeV, respectively. The absorbed dose (i.e., the total "irradiation" time of the DMD in the beam) was increased in steps of 2 krad or more. This is the equivalent dose after eight months on orbit at L2. The functionality of the DMDs was examined during the intervals between each irradiation step by exercising the DMD with a series of patterns. The irradiation sequences are described in Secs. 2.4.1–2.4.3. The measures of the DMD postirradiation operability are described in Secs. 3.2 and 3.4.

2.1 *Proton Irradiation Facility*

To undertake proton testing of DMDs, 48 h were allocated at the Lawrence Berkeley National Laboratory (LBNL) 88 in. cyclotron. The testing was completed in cave 4A where the beam-line provided energies between 35.0 and 49.9 MeV. Electronic attenuators allowed control of the beam to a desired flux rate. Only three beam energies were utilized because the facility change time was between 5 and 8 h. A considerable amount of the time between irradiation increments was required to complete the optical characterization of the DMD.

2.2 *Irradiation Test Setup*

Figure 4 shows the beam-line experiment. The protons from the cyclotron exit the port as shown in A. The ionization chamber (B) is located after the beam exit port. A 2-in. aluminum aperture plate (C) is employed to collimate the proton beam as the DMD (I) under test has a 0.7 in. diagonal. This aperture size is sufficient to permit the entire DMD active area and package to be uniformly irradiated. The DMD drive electronics (Discovery 4000 Kit) is shielded using. 0.75 in. aluminum plate (H) and therefore is not irradiated, to evaluate the true proton irradiation tolerance of the DMD itself. The DMD was placed as close as possible to the beam exit port, but with sufficient room to place the camera fixture. To limit systematic uncertainties and facilitate comparison

Downloaded From: http://opticalengineering.spiedigitallibrary.org/ on 04/25/2016 Terms of Use: http://spiedigitallibrary.org/ss/TermsOfUse.aspx

Fig. 4 Parts of the experimental apparatus are as follows: (A) is the proton beam-line exit port, (B) ionization chamber, (C) aluminum aperture plate, (D) high speed CCD camera, (E) a macro lens, (F) LED light source, (G) kinematic mount, (H) 0.75 in. aluminum shielding for the drive electronics, and (I) test DMD.

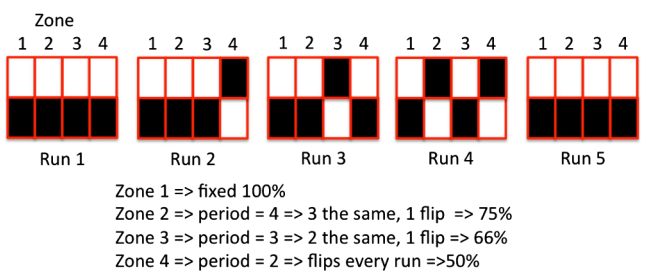

Fig. 5 Five sequential DMD run patterns are shown here. Each zone is composed of 248 columns of DMD mirrors. For run one the top half of the DMD mirrors are on, and the bottom half are off. During run two, the mirrors are flipped in zone four. Next, for run three, the mirrors in zone three are flipped. This sequence continues for each irradiation step. This set of patterns is used to investigate the mirrors duty-cycle during proton irradiation. For the zones one to four, the duty-cycles tested were 100%, 75%, 66%, and 50%. Mirrors in zone one were in the same position for each irradiation. Mirrors in zone four alternated positions every other irradiation step.

between subsequent irradiation runs, the DMD is not removed from the test bench or unpowered for the duration of the test procedures. After each irradiation step, a CCD camera (D) and 50 mm C-mount lens (E) is placed in the beam-line looking at the DMD. This allows the DMD to be re-imaged onto the camera. A kinematic magnetic mount (G) serves as the repeatable mounting fixture for this camera and light source (F). The lens aperture is set to $f/4$ for the duration of the experimental data collection. An LED light source is used to uniformly illuminate the active area of the DMD during the imaging process.

2.3 *Optical Test Procedure*

The goal of the optical test procedure was to determine which mirrors in the DMD array remained fully functional at increasing dose levels. Operational mirrors were defined as mirrors that would flip to both stable states. Nonfunctional mirrors were either stuck in one position, or failed to flip towards the CCD camera. Mirrors that stick would be permanently attached to the substrate in either the "on" position or the "off" position. Mirrors that fail to flip are mirrors in the central neutral position due to, e.g., a broken hinge or electrodes that fail to load the proper voltages. The optical test procedure for the DMD had two sets of patterns. One set of "run" patterns was sent to the DMD for use during the proton irradiation (Fig. 5). A second set of "test" patterns (Fig. 6) was used to check the functionality of each individual mirror after irradiation.

The purpose of the first set of run patterns was to have the mirrors latched in one of the two stable positions for an irradiation, much like they would see on orbit. It was of interest to determine if any mirrors flipped during the irradiation, so a simple procedure was devised. The run pattern was loaded into the DMD and an image was taken with the CCD camera. After the DMD was irradiated, a second image was taken. By subtracting these two images, the mirrors that flipped during the irradiation were detected. Next, the same run pattern was reloaded and another image was taken. This procedure is illustrated in Fig. 7. The second image was used to verify that flipped mirrors would return to their programmed state

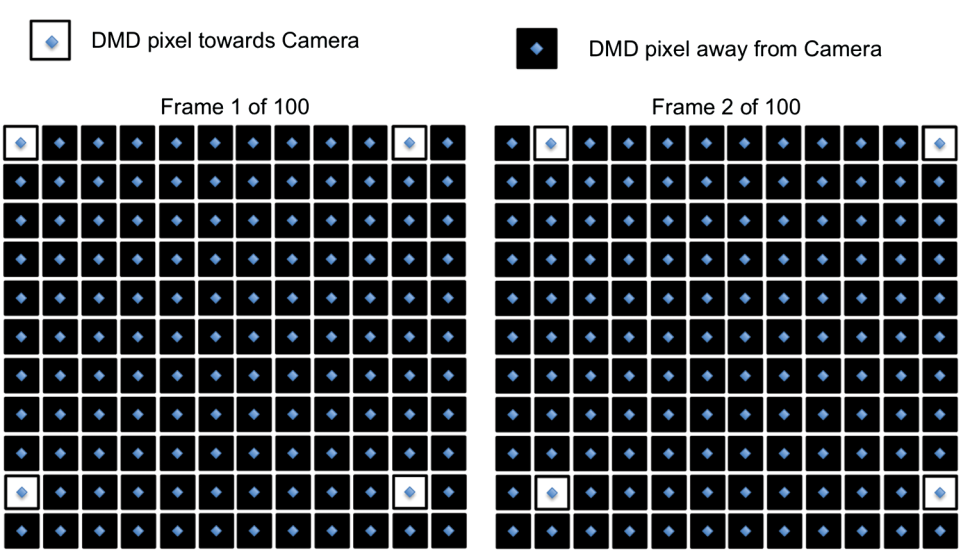

Fig. 6 Two DMD test patterns are shown here. One mirror per 10×10 subarray is facing the CCD camera. This subarray is tiled across the DMD in its entirety. After a series of 100 of these test frames are loaded and imaged, the optical test procedure is complete.

Downloaded From: http://opticalengineering.spiedigitallibrary.org/ on 04/25/2016 Terms of Use: http://spiedigitallibrary.org/ss/TermsOfUse.aspx

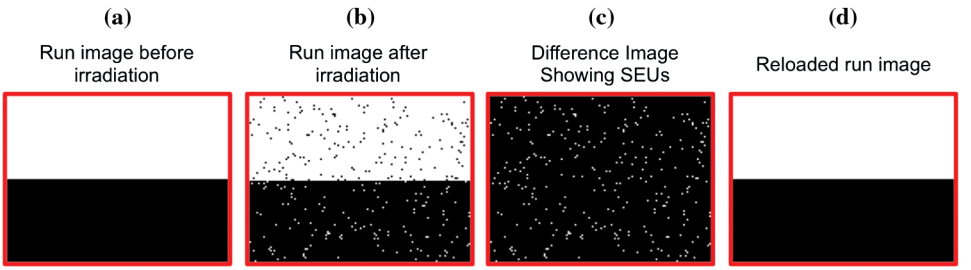

Fig. 7 (a) Run pattern was loaded into the DMD prior to the proton irradiation and an image was captured with the camera. (b) Image was captured with the CCD camera after irradiation. Mirrors that flipped during the irradiation look dark in the top half of the array and bright in the bottom half to the array in this example. (c) $|a - b|$ shows the locations of all of the flipped mirrors in the irradiation. (d) Same run pattern was reloaded into the DMD to ensure all mirrors went back to their programmed state.

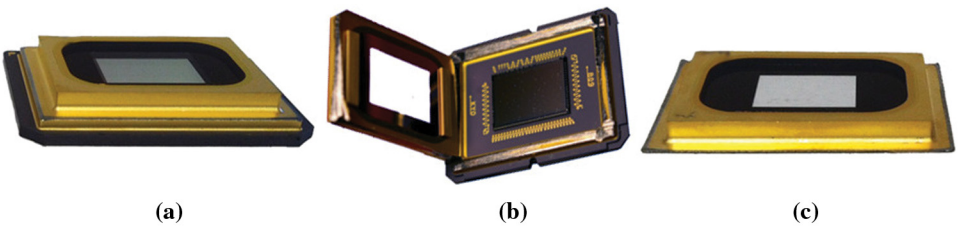

Fig. 8 (a) Original DMD package. (b) Kovar metal frame and window are in the process of being removed from the DMD package. (c) Kovar frame and window are separated from the DMD package.

after reloading the DMD memory. The run pattern was broken up into four duty-cycle zones. Each zone was composed of 248 columns on the DMD. Duty-cycle is defined as the percent of time a given mirror is in one state for the irradiations versus the opposite state. To determine if the mirror's duty-cycle was a significant parameter, the run pattern was changed between subsequent irradiation steps. In zone one, the mirrors were kept in the same state for all irradiation steps. The zone four mirrors changed position at each subsequent irradiation step. For the zones one to four, the duty-cycles tested were 100%, 75%, 66%, and 50%. The test pattern was latched and held for the duration of one irradiation.

After the run pattern images were taken, a separate set of "test" patterns (Fig. 6) was sent to the DMD. The first DMD test pattern had all of the mirrors along the perimeter orientated towards the CCD camera. An image was then taken with the CCD camera. This enabled the calibration of spatial correspondence between mirrors and CCD pixels. The DMD test pattern was then broken up into 10×10 blocks. A single DMD mirror, from each 10×10 block, faced the camera. This 10×10 blocking was repeated across the entire DMD. The CCD camera captured the series of 100 test patterns, so that each individual mirror in the DMD faced the CCD camera in exactly one image. This procedure was repeated at each irradiation step. This same testing procedure was performed at each of the three energies. The images were post-processed and truth maps were constructed after the testing was completed.

2.4 *Irradiation Sequence*

2.4.1 *Energy #1 (Beam—34.0 MeV device—21.0 MeV) DMD serial number 140508*

The initial set of tests was conducted with the beam energy tuned to 34 MeV. Prior to irradiating devices, the beam had to be optimized for uniformity across the beam aperture. The distance between the DMD and the aperture plate was port was approximately 12 in. Over this distance, the beam divergence was negligible. The beam divergence was measured by placing a piece of film at the DMD test location and measuring the diameter (2 in.) which was the same as the collimator plate. Gafcrhomic RTAQ2[17] film recorded the beam uniformity at the DMD sample location. The film was scanned using an on-site densitometer. This process was repeated until the beam was adjusted to be within the desired uniformity (approximately 1% uniformity across the DMD).

Prior to traveling to LBNL, the top kovar metal frame with window was removed from four surplus DMDs. This

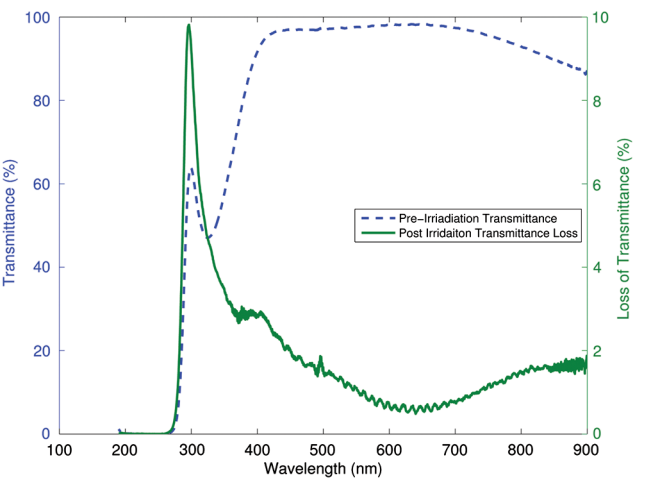

Fig. 9 (Left *y*-axis) Average preirradiation transmittance of the DMD windows. (Right *y*-axis) Average postirradiation transmittance loss for a 20 krad dose. These values are for a single-pass measurement through the window.

Downloaded From: http://opticalengineering.spiedigitallibrary.org/ on 04/25/2016 Terms of Use: http://spiedigitallibrary.org/ss/TermsOfUse.aspx

process is illustrated in Fig. 8. The bottom portion of the package with DMD silicon was discarded. These four sets of window frames were used to determine if the glass transmission changed after proton irradiation. One of the DMD window frames was then irradiated with 34 MeV protons to a dose of 20 krad with the beam incident normal to the window. The window transmittance results are shown in Fig. 9, and the results are presented in Sec. 3.1.

After the first window frame had been irradiated, a powered and biased DMD was tested at 34 MeV (21 MeV incident at the silicon). All of the DMDs were irradiated with the proton beam incident normal to the window. Before irradiation, the baseline DMD functionality was validated using an optical test procedure as is described in Sec. 2.3. The DMD run one pattern was loaded into the DMD. Next, the full surface of the DMD was irradiated to 2 krad incident. The optical test procedure (Sec. 2.3) was then performed. For each run, the loaded run pattern (Fig. 5) was modified to test the influence of duty cycle. This was repeated until run 10, where each run corresponded to an additional 2 krad incident dose. After run 10 the irradiation dose step was increased to 5 krad incident, and three additional runs were performed. The 34 MeV run log is shown in Table 2.

2.4.2 *Energy #2 (Beam—44.2 MeV silicon—34.5 MeV) DMD serial number 140507*

Next, the beam energy was tuned to 44.2 MeV. The same beam uniformity measurements were taken with the Gafchromic film. The second DMD window was irradiated to 20 krad. After the window was irradiated, the second DMD was placed in the beam-line using the same control electronics to drive the DMD. A preirradiation optical scan was completed. Then, a run pattern (Fig. 5) was loaded into the DMD. The DMD was irradiated to a 4 krad incident dose, and a post irradiation optical test was completed (Sec. 2.3). The proton energy at the DMD silicon was 34.5 MeV. The modified run image for run two was then loaded into the DMD. This procedure was repeated until run six at which time the irradiation dose increment was changed to 5 krad incident. The 44.2 MeV run log is shown in Table 3. After the final irradiation increment and prior to the removal of this DMD from the beam-line, an unknown but substantial additional proton dose irradiated this device due to a beam-line control malfunction.

2.4.3 *Energy #3 (Beam—49.3 MeV silicon—40.9 MeV) DMD serial number 140106*

To test the final device, the beam was tuned to 49.3 MeV. At the highest energies it was more difficult to tune the cyclotron, and it therefore involved the longest downtime. The third window was irradiated to a dose of 20 krad. The preirradiation test was done on the third DMD. The run pattern (Fig. 5) was loaded into the DMD. It was irradiated to a 4 krad incident dose. The optical test procedure was then repeated on this DMD at each irradiation step. The step sizes were kept constant at 4 krad incident until run six, at which

Table 2 34 MeV run log for DMD serial number 140508. The energy at the DMD silicon is 21.0 MeV.

#	(p^+/cm^2 s)	Incremental fluence (p^+/cm^2 s)	(p^+/cm^2)	Incremental dose (krad)	Integral dose (krad)	Silicon dose (krad)	Irradiation time (s)
1	5.3×10^{7}	9.07×10^{9}	9.1×10^{09}	2.0	2.0	2.74	172
2	5.4×10^{7}	9.07×10^{9}	1.8×10^{10}	2.0	4.0	5.48	169
3	5.3×10^{7}	9.08×10^{9}	2.7×10^{10}	2.0	6.0	8.22	173
4	5.5×10^{7}	9.08×10^{9}	3.6×10^{10}	2.0	8.0	10.96	166
5	5.6×10^{7}	9.08×10^{9}	4.5×10^{10}	2.0	10.0	13.70	163
6	5.8×10^{7}	9.08×10^{9}	5.4×10^{10}	2.0	12.0	16.44	157
7	5.5×10^{7}	9.09×10^{9}	6.4×10^{10}	2.0	14.0	19.18	164
8	5.4×10^{7}	9.08×10^{9}	7.3×10^{10}	2.0	16.0	21.92	168
9	5.1×10^{7}	9.11×10^{9}	8.2×10^{10}	2.0	18.0	24.67	179
10	4.8×10^{7}	9.10×10^{9}	9.1×10^{10}	2.0	20.0	27.42	189
11[a]	5.1×10^{7}	2.25×10^{10}	1.1×10^{11}	5.0	25.0	34.21	445
12[b]	4.6×10^{7}	2.25×10^{10}	1.4×10^{11}	5.0	30.0	41.01	493
13[c]	4.7×10^{7}	2.25×10^{10}	1.6×10^{11}	5.0	34.9	47.81	476

[a]Started to see sticking mirrors in zone 1.
[b]Started to see additional sticking and nonfunctional mirrors in other zones.
[c]Effects continued across all four zones.

Downloaded From: http://opticalengineering.spiedigitallibrary.org/ on 04/25/2016 Terms of Use: http://spiedigitallibrary.org/ss/TermsOfUse.aspx

Table 3 44.2 MeV run log for DMD serial number 140507. The energy at the DMD silicon is 34.5 MeV.

#	$(p^+/\text{cm}^2\,\text{s})$	Incremental fluence $((p^+/\text{cm}^2))$	(p^+/cm^2)	Incremental dose (krad)	Integral dose (krad)	Silicon dose (krad)	Irradiation time (s)
1	8.5×10^7	2.30×10^{10}	2.3×10^{10}	4.1	4.1	4.87	271
2	7.5×10^7	2.30×10^{10}	4.6×10^{10}	4.1	8.1	9.75	305
3	8.4×10^7	2.30×10^{10}	6.9×10^{10}	4.1	12.2	14.62	273
4	8.6×10^7	2.30×10^{10}	9.2×10^{10}	4.1	16.2	19.49	269
5	8.4×10^7	2.30×10^{10}	1.2×10^{11}	4.1	20.3	24.36	274
6	7.3×10^7	2.87×10^{10}	1.4×10^{11}	5.1	25.4	30.43	391
7[a]	7.3×10^7	2.87×10^{10}	1.7×10^{11}	5.1	30.4	36.49	392
8	7.1×10^7	2.86×10^{10}	2.0×10^{11}	5.1	35.5	42.56	404

[a]Started to see effects in zone 1. After dose increment 8, this DMD received an extra unknown dose due to beam-line control malfunction.

point the step size was changed to 5 krad incident. The 49.3 MeV run log is shown in Table 4.

3 Results

3.1 *Postirradiation Window Transmittance Loss*

After irradiating the window frames to 20 krad, they became activated, and remained at LBNL for several weeks until they cooled to background level. After the windows were returned to Rochester Institute of Technology (RIT), their transmittance and that of an unirradiated control window frame were measured on Shimadzu Spectro-Photometer 2100 – UV. Figure 9 shows the transmittance measurements, with a loss of 1% to 3% in the range 3.500 to 9.000 Å, and a peak up to 10% at 3000 Å. The windows were then remeasured on a separate instrument, a J. A. Whoollam Variable Angle Spectroscopic Ellipsometer to validate these results. It is well known that borosilicate glass will yellow after being exposed to high-energy protons,[18] and our results illustrate this effect. These results are for a single-pass measurement, so the total loss of transmittance would be the square of this value. An alternative window material such as magnesium fluoride, which does not yellow as readily, could be used in the DMD package. However, the coefficient of thermal expansion of the borosilicate window is best matched to the entire DMD package.

Table 4 49.3 MeV run log for DMD serial number 140106. The energy at the DMD silicon is 40.9 MeV.

#	$(p^+/\text{cm}^2\,\text{s})$	Incremental fluence (p^+/cm^2)	(p^+/cm^2)	Incremental dose (krad)	Integral dose (krad)	Silicon dose (krad)	Irradiation time (s)
1	5.0×10^7	2.40×10^{10}	2.4×10^{10}	4.0	4.0	4.45	479
2	4.5×10^7	2.40×10^{10}	4.8×10^{10}	4.0	8.0	8.90	537
3	4.1×10^7	2.43×10^{10}	7.2×10^{10}	4.0	12.0	13.40	597
4	3.9×10^7	2.40×10^{10}	9.6×10^{10}	4.0	16.1	17.85	611
5	3.6×10^7	2.40×10^{10}	1.2×10^{11}	4.0	20.1	22.30	672
6[a]	3.4×10^7	3.00×10^{10}	1.5×10^{11}	5.0	25.1	27.87	890
7[b]	3.3×10^7	3.00×10^{10}	1.8×10^{11}	5.0	30.1	33.43	902
8[c]	3.0×10^7	3.00×10^{10}	2.1×10^{11}	5.0	35.1	38.99	995

[a]Started to see effects in zone 1.
[b]Global effects continue, and some mirrors recover by the end of optical characterization.
[c]Most of array is nonfunctional.

Downloaded From: http://opticalengineering.spiedigitallibrary.org/ on 04/25/2016 Terms of Use: http://spiedigitallibrary.org/ss/TermsOfUse.aspx

3.2 *Postirradiation DMD Functionality*

The results of the optical tests at each irradiation step are shown in Fig. 10. The percentages of operational mirrors are shown as a function of proton dose. At all three tested energies, the DMDs withstood a TID of approximately 30 krad. After the irradiation procedure at each energy was completed, the mirrors were exercised using an alternating checkerboard pattern for several thousand cycles. By rapidly re-landing mirrors, mirrors that previously could only land in one position were able to land in both states. Since the DMDs can flip mirrors at 20 kHz, this operation requires a fraction of a second. For the DMD irradiated with 21.0 MeV protons, 90% of the mirrors immediately recovered. Exercising was not as effective for the 49.9 MeV device. The results of exercising the DMD after 34.5 MeV protons are ambiguous because of the substantially large dose this DMD received after a beam-line malfunction. Additionally there was little change after exercising the DMD mirrors at the highest beam energy. The same three DMDs were then tested again after a six-month room temperature anneal. Six months was the time it took for the activated DMDs to be returned from LBNL and retested in the laboratory. Most of the mirrors fully recovered after this anneal (Table 5). It is likely that an accelerated anneal could be done at elevated temperatures with similar results.

As discussed previously, the DMD was segmented into four separate duty-cycle zones in each of the run patterns. The zone one mirrors were the first to fail in all three energies. At higher TID the mirrors in zones two and three also failed. For all three proton energies (trials), the mirrors in zone four (the 50% duty-cycle) operated to the highest TID level. To characterize this effect more precisely, smaller dose increments would be needed.

3.3 *Duty Cycle Effect*

The underlying cause for this apparent duty-cycle effect is unknown, but may be mechanical in nature. Possibly, when the mirror is latched in one state and the torsional hinge is irradiated, new defects are created in the hinge. These defects reduce the stress in the latched hinge, and once bias is removed from this mirror, the mirror no longer returns to its flat state. A related effect, seen when DMDs are used in projectors operated at elevated temperatures, called "hinge memory" has been discussed.[19] The two higher energies that used even larger dose increment began exhibiting performance issues at slightly lower TID levels. This indicates that the DMD has an apparent dose-rate effect, and that both the irradiation rate and TID are important in assessing the effect of protons on DMD performance. The exercising and duty-cycle effects observed indicate the testing conditions were harsh and unrealistic for several reasons. A minimum increment 2 krad was used during our testing. This 2 krad dose corresponds to the radiation dose the DMD would obtain after several months on orbit. On orbit, it may be beneficial to optimize DMD operation to extend their life. Operationally, one can envision to exercise the DMD in idle mode, switching them at high frequency (10 kHz or more, as designed) between their on/off positions, each time an observation is not being carried out, like e.g., during telescope moves and in general when the light detectors (CCD or IR) are also in idle mode.

3.3.1 *Heating effects*

An alternate explanation for the hinge memory effect relates to hinge heating. This has been discussed previously.[20] A worst case heating scenario due to proton kinetic energy transfer assumes all the proton kinetic energy during an irradiation step is converted into thermal energy. The change in

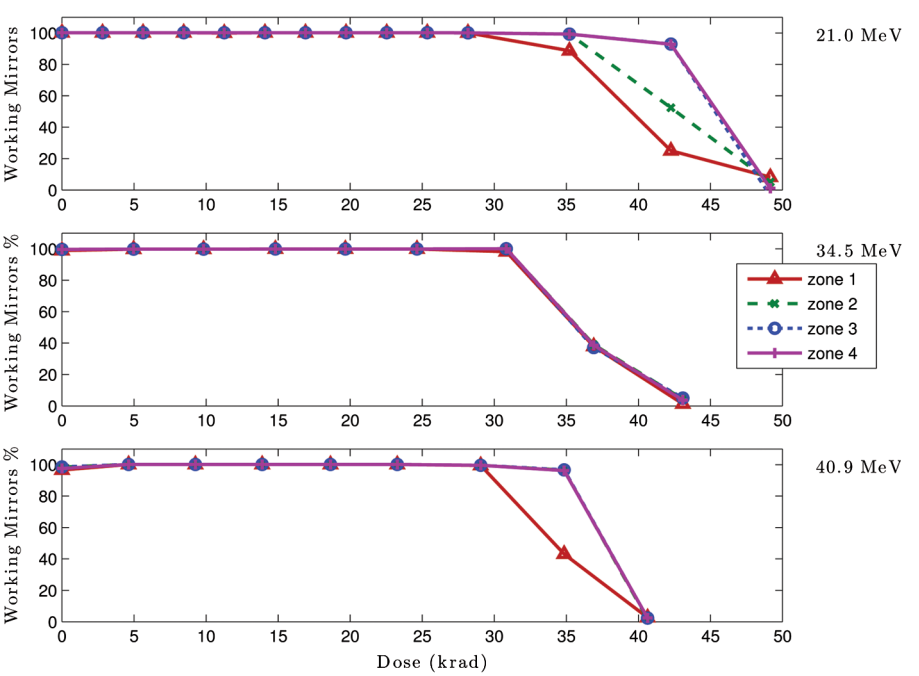

Fig. 10 Percentage of working mirrors is plotted versus dose in krad. Note, the 34.5 MeV device was irradiated to an additional unknown dosage level after the last data point.

Downloaded From: http://opticalengineering.spiedigitallibrary.org/ on 04/25/2016 Terms of Use: http://spiedigitallibrary.org/ss/TermsOfUse.aspx

Table 5 The postexposure DMD operability is shown here. Exercising was beneficial for the mirrors at the lowest energy 21.0 MeV.

	After irradiation (%)	After exercising (%)	After six month room temperature anneal (%)
21.0 MeV			
Zone 1	5.0	26.7	99.98
Zone 2	2.9	86.9	100
Zone 3	0.0	95.5	100
Zone 4	1.2	95.7	100
34.5 MeV			
Zone 1	1.6	–	79.72
Zone 2	5.8	–	80.2
Zone 3	6.6	–	90.4
Zone 4	5.2	–	96.0
40.9 MeV			
Zone 1	3.2	3.2	99.99
Zone 2	3.1	3.1	100
Zone 3	3.7	3.7	100
Zone 4	2.7	2.7	100

temperature can be calculated from the specific heat of aluminum, target mass of the DMD, and energy absorbed from the incident 55 MeV protons. A δT much less than 1°C is obtained. Comparatively when the DMD is used in a high output commercial projector, a thermal load ($\delta T > 10$°C) is placed on the DMD with minimal effects. Thus, a thermal explanation for the mirrors becoming stuck does not seem viable.

3.3.2 *Trapped oxide charge (dielectric charging)*

Another possible cause of sticking mirrors is trapped charge in DMD oxides. Metal oxide field effect transistors (MOSFET) are very sensitive to trapped charge in insulating oxide layers.[21] The types of trapped charge affect NMOS and PMOS devices differently. As a charged particle passes through the oxide layer, the radiation creates electron hole pairs. On average, one charge pair is produced[22] for each 17 eV of energy absorbed by the material. The only trapped charge that is important for the MEMS portion of the mirrors is unshielded trapped charge. If there are regions of the DMD that have oxide without metal overlapping them, this can cause the mirror actuation voltage to change. Without being able to directly test the CMOS

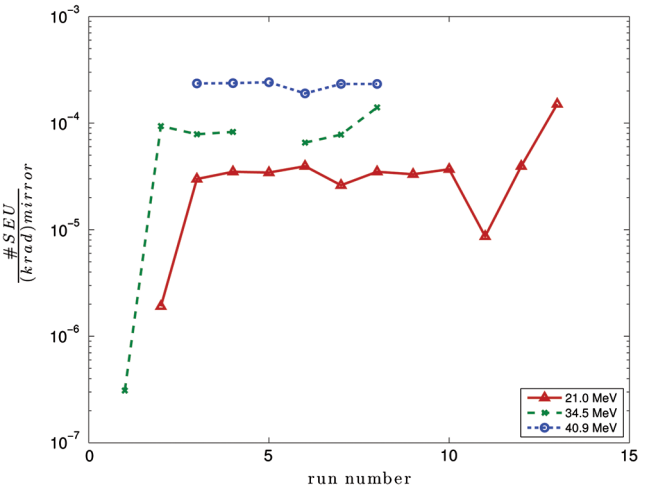

Fig. 11 Number of upsets per mirror versus run number at each proton energy. For example, 10^{-4} SEU/(krad)mirror $\times$ (1024$\times$ 768 mirrors) $\times$ 6.6 krad = 519(SEU/5 years) = 103.8(SEU/year) = 0.28(SEU/Day). This DMD would have one upset mirror every four days of operation during a five-year mission at L2.

memory, it is difficult to determine if the trapped charge is present in the DMD's CMOS transistors, or if the trapped charge occurs in its MEMS spacer oxide layers in the superstructure. Trapped charge in either of these locations could cause mirrors to no longer function. Various different types of MEMS devices have been shown to be sensitive to trapped charge[23] in these locations due to the nature of their electrostatic design.[24]

3.4 *(Mirror Upsets During Irradiation) Single Event Upsets*

During proton irradiation, some mirrors flipped from their programmed position to the opposite position (from $\pm 12°$ to $\mp 12°$). Figure 11 shows the number of such upsets as a function of dose. This is likely caused by upsets in the CMOS memory. The upset was nondestructive and was correctable by reloading the DMD memory. These types of upsets are well characterized in SRAM and are often called a SEU. These upsets were present in all proton energies tested. As the proton energy increased, the number of upsets per dose increment was more frequent. This is likely because the protons are not causing the upsets by direct ionization. The protons, upon interaction with the target material, create heavier secondary particles. These heavier secondary particles, which correspondingly have a higher LET than the original protons, are likely the reason for an increase in upsets as the beam energy increases. At each energy and dose, when the DMD memory was reloaded, all of the flipped mirrors returned to their programmed state. The upset rate is approximately 10^{-4} [SEU/(krad)mirror]. Since there are 1024×768 mirrors and the dose for five-years is 6.6 krad, 519(SEU/5 years) upsets would occur during the five-year mission. On average at L2, this DMD would have one mirror upset every four days.

The cumulative upsets were calculated for all of the irradiation steps. The upsets per mirror are shown as a function of fluence (# of protons) in Fig. 12. The last irradiation increment resulted in an increased number of upsets at each of the energies. A line was fit to each of the datasets corresponding

Downloaded From: http://opticalengineering.spiedigitallibrary.org/ on 04/25/2016 Terms of Use: http://spiedigitallibrary.org/ss/TermsOfUse.aspx

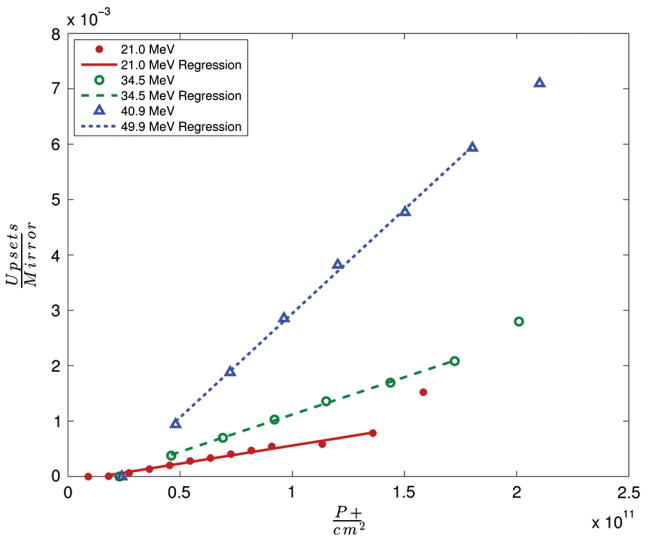

Fig. 12 Slope represents the SEU cross-section.

Table 6 SEU cross-section values are presented here for each proton energy.

Energy (MeV)	Cross-section (cm^2/mirror)
21.0	6.525×10^{-15}
34.5	1.346×10^{-14}
40.9	3.755×10^{-14}

to the three energies. The point from the last irradiation increment was not included in the regression because the nature of the SEU phenomenon changes. This effect is likely the point at which some critical threshold of trapped charge has been reached in the SRAM below the DMD. The slopes of this line, proportional to the SEU cross-section, are tabulated in Table 6. With this information, the probability of a mirror flipping on orbit during a spectrometer integration time can be calculated. The number of upsets and cross-sections are comparable to other SRAM memory devices.[25]

4 Conclusion

A test procedure was developed to characterize proton irradiated DMDs at three different proton energies. During irradiation two effects were observed that affected the performance of the device. The DMDs were 100% functional to a TID of 30 krad. For higher doses, it appears that the duty-cycle of the mirrors (i.e., the ratio of time the mirror is latched in one state versus the opposite latched position) during the irradiation is important. Additionally, the proton flux rate also appears to be a significant factor in determining DMD performance above 30 krad. The DMD failures are believed to be caused by trapped charges in oxide layers, either in the CMOS memory transistors, or in the MEMS super-structure itself. Future work will test additional electrical parameters to determine if the failure mechanisms are within the CMOS memory or in the MEMS superstructure. Operationally, there were benefits from exercising the mirrors to avoid duty-cycle effects, and thermal annealing seems to cure most of the damage not recovered by exercising the mirrors.

Some mirrors flipped from their programmed position to their opposite position during proton irradiation. This is a type of SEU caused by CMOS memory upsets. The calculated SEU rates and corresponding upset cross-sections agreed with those quoted for other SRAM devices fabricated with similar design rules.

While DMDs with the shielding from their package shielding can withstand a five-year mission with a 2× margin of safety and a 4.5× margin of safety if 100 mil of space-craft shielding is used. Overall, DMDs appear to function well in a proton radiation environment and should be considered as a candidate for a slit mask on a future space mission.

References

1. L. Hornbeck, "Current status of the digital micromirror device (DMD) for projection television applications," in *Electron Devices Meeting, 1993. IEDM'93, Technical Digest., International*, pp. 381–384, IEEE, Washington, DC (1993).
2. M. Douglass, "DMD reliability: a MEMS success story," *Proc. SPIE* **4980**, 1–11 (2003).
3. R. D. Meyer, "RITMOS: a micromirror-based multi-object spectrometer," *Proc. SPIE* **5492**, 200–219 (2004).
4. J. W. MacKenty, "IRMOS: an infrared multi-object spectrometer using a MEMS micro-mirror array," *Proc. SPIE* **4841**, 953–961 (2003).
5. H.-J. Ziock et al., "Temperature dependence of the radiation induced change of depletion voltage in silicon pin detectors," *Nucl. Instrum. Methods Phys. Res. Sect. A* **342**(1), 96–104 (1994).
6. S. Barden and T. Armandroff, "Performance of the WIYN fiber-fed MOS system: Hydra," *Proc. SPIE* **2476**, 56–67 (1995).
7. R. L. Davies et al., "GMOS: the GEMINI multiple object spectrographs," *Proc. SPIE* **2871**, 1099–1106 (1997).
8. A. Kutyrev et al., "Programmable microshutter arrays for the JWST NIRSpec: optical performance," *IEEE J. Sel. Topics Quant. Electron.* **10**(3), 652–661 (2004).
9. F. Zamkotsian, "Dmd-based mos demonstrator on galileo telescope," *Proc. SPIE* **7735**, 77356E (2010).
10. M. Robberto et al., "Applications of dmds for astrophysical research," *Proc. SPIE* **7210**, 72100A (2009).
11. F. Zamkotsian et al., "DMD chip space evaluation for ESA's EUCLID mission," *Proc. SPIE* **7596**, 75960E (2010).
12. H. Shea, "Effects of radiation on MEMS," *Proc. SPIE* **7928**, 79280E (2011).
13. D. Heynderickx et al., "ESA's space environment information system (SPENVIS)—a WWW interface to models of the space environment and its effects," in *Proc. 38th Aerospace Sciences Meeting and Exhibit*, Vol. 371, p. 475, AIAA (2000).
14. M. Xapsos et al., "Space environment effects: model for emission of solar protons (ESP): cumulative and worst case event fluences," NASA STI/Recon Technical Report N, 21507 (1999).
15. J. Barth, J. Isaacs, and C. Poivey, "The radiation environment for the next generation space telescope," NGST Project, Internal Document (1999).
16. "James Ziegler—SRIM & TRIM," Lulu Press Co., Morrisville, North Carolina, http://www.srim.org/SRIM%20Book.htm (20 Jan 2012).
17. "Gafchromic rtqa2," Ashland Inc., http://www.gafchromic.com/ (10 April 2012).
18. S. Pellicori, E. Russell, and L. Watts, "Radiation induced transmission loss in optical materials," *Appl. Opt.* **18**(15), 2618–2621 (1979).
19. M. Douglass, "Lifetime estimates and unique failure mechanisms of the digital micromirror device (DMD)," in *Proc. 36th Annual IEEE Int. Reliability Physics Symp.*, pp. 9–16, IEEE, Reno, Nevada (1998).
20. A. Sontheimer, "Digital micromirror device (DMD) hinge memory lifetime reliability modeling," in *Proc. 40th Annual Reliability Physics Symp.*, pp. 118–121, IEEE, Plano, Texas (2002).
21. P. McWhorter and P. Winokur, "Simple technique for separating the effects of interface traps and trapped-oxide charge in metal-oxide-semiconductor transistors," *Appl. Phys. Lett.* **48**(2), 133–135 (1986).
22. J. Benedetto and H. Boesch, "The relationship between 60co and 10-kev x-ray damage in mos devices," *IEEE Trans. Nucl. Sci.* **33**(6), 1317–1323 (1986).
23. L. Edmonds, G. Swift, and C. Lee, "Radiation response of a MEMS accelerometer: an electrostatic force," *IEEE Trans. Nucl. Sci.* **45**(6), 2779–2788 (1998).
24. T. Miyahira et al., "Total dose degradation of MEMS optical mirrors," *IEEE Trans. Nucl. Sci.* **50**(6), 1860–1866 (2003).
25. E. Petersen, "The seu figure of merit and proton upset rate calculations," *IEEE Trans. Nucl. Sci.* **45**(6), 2550–2562 (1998).

Downloaded From: http://opticalengineering.spiedigitallibrary.org/ on 04/25/2016 Terms of Use: http://spiedigitallibrary.org/ss/TermsOfUse.aspx

Kenneth Fourspring has been a PhD student at Rochester Institute of Technology, Rochester, New York, since 2009. He is a NASA Graduate Research Student Research (GSRP) fellow. In 2008, he graduated with a BS in microelectronic engineering at Rochester Institute of Technology.

Zoran Ninkov is a professor at the Rochester Institute of Technology, Rochester, New York. He received his BSc 1st Class Honors in physics at the University of Western Australia, Crawley, WA, in 1978, his MSc degree in physical chemistry from Monash University in 1981, and his PhD in astronomy from the University of British Columbia, Vancouver, BC. His research interests are in the area of instrumentation development, detector testing, and MEMS devices.

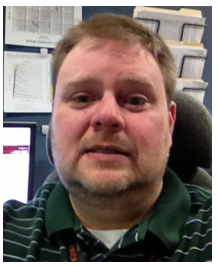

Bryan C. Fodness is a graduate student at Rochester Institute of Technology, Center for Imaging Science, Rochester, New York. He has spent 10 years working in the space environments and radiation effects field. He plans to receive his MS in imaging science in 2014 and in 1999 graduated with a BS in physics from Bloomsburg University of Pennsylvania, Bloomsburgh, Pennsylvania.

Massimo Robberto is AURA scientist at the Space Telescope Science Institute (STScI) in Baltimore, Maryland, working within the Instrument Division as instrument scientist and technical lead for NIRCAM, the near-infrared camera for the James Webb Space Telescope. Before joining STScI, he has beep part of the science staff of the Turin Astronomical Observatory (Italy), Max Planck Institute fuer Astronomie (Heidelberg, German) and the European Space Agency. His main expertise is the concept, development and operations of new infrared instrumentation, both for ground and space astronomy.

Sally Heap has been an astronomer at NASA's Goddard Space Flight Center since 1969.

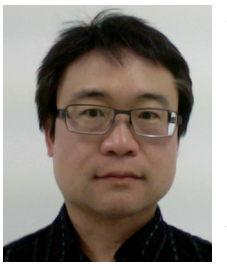

Alex G. Kim is a staff scientist in the Physics Division of Lawrence Berkeley National Laboratory. His research interests are in type Ia supernova cosmology and is currently participates in several experiments: the Nearby Supernova Factory 2, Dark Energy Survey, Large Synoptic Survey—Dark Energy Science Collaboration, and Euclid Consortium. He received his BS in physics from the University of Michigan, Ann Arbor, Michigan, in 1991, and his doctorate in physics from the University of California, Berkeley, California, in 1996.

Downloaded From: http://opticalengineering.spiedigitallibrary.org/ on 04/25/2016 Terms of Use: http://spiedigitallibrary.org/ss/TermsOfUse.aspx